An experimental investigation of the ignition properties of low temperature combustion in an optical engine

by

Bradley Thomas Zigler

A dissertation submitted in partial fulfillment
of the requirements for the degree of
Doctor of Philosophy
(Mechanical Engineering)
in The University of Michigan
2008

Doctoral Committee:

Professor Margaret S. Wooldridge, Chair
Professor Dionissios N. Assanis
Professor James F. Driscoll
Associate Research Professor Zoran S. Filipi
Steven T. Wooldridge, Ford Motor Company

To my wife, Lauren.

ACKNOWLEDGEMENTS

This dissertation represents the culmination of several years of exciting discovery and growth for me. My foremost appreciation goes to Professor Margaret Wooldridge. My initial meetings with her convinced me to select her laboratory research group and the University of Michigan for my Ph.D. studies. Nearing the end of this process, I remain convinced I made the right choice of advisor and institution. Professor Wooldridge has shared vast experience, invaluable guidance, critical insight, and constant positive support during my studies and research. I am proud to say I am a colleague in her research group.

I would also like to thank my other committee members: Professor Dennis Assanis, Professor James Driscoll, Associate Research Professor Zoran Filipi, and Dr. Steven Wooldridge. Their review of my research provides me insightful and focused feedback. I have enjoyed their continual beneficial input along the way.

I am also very grateful for endless contributions help from my laboratory colleagues. I am fortunate to have studied, shared, and worked with such a talented group of individuals, including: Dr. Michael Donovan, Dr. Tiffany Miller, Dr. Xin He, Travis Palmer, Steve Walton, Smitesh Bakrania, James Wiswall, Carlos Perez, Dimitris Assanis, Liz Perez, Darshan Karwat, and Kyeongmin Kim.

I have also benefited greatly from financial, material, and technical support from various organizations and individuals. First, this research project would not have been possible without Dr. Steven Wooldridge's support and efforts on behalf of the

Ford Motor Company - Ford Research and Advanced Engineering. This valuable collaborative relationship resulted in the generous donation of the optical research engine used as the foundation of the research facility constructed in support of the research documented here. I also benefited from the University of Michigan Corlett Fellowship, which allowed me the freedom to focus on my research. The U.S. Department of Energy - HCCI University Consortium also provided valuable financial assistance and an outstanding forum for regular peer review of my research progress. I am also indebted to the National Science Foundation for their financial support of this research and the University of Michigan - Horace H. Rackham School of Graduate Studies for providing travel support to allow me to continually publish and present my research work at conferences.

My thanks and appreciation also go to my parents, Thomas and Virginia Zigler, who have always proudly supported me and understood my decision to pause my corporate career and pursue my Ph.D. research studies. Finally, I would like to thank my wife, Lauren Ramsay, for her love and unwavering support during this process. Lauren's dedication to her own Ph.D. studies has also served as a great source of inspiration.

TABLE OF CONTENTS

LIST OF FIGURES

Figure

LIST OF TABLES

Table

LIST OF APPENDICES

Appendix

ABSTRACT

An experimental investigation of the ignition properties of low temperature combustion in an optical engine

by

Bradley Thomas Zigler

Chair: Margaret S. Wooldridge

Homogeneous charge compression ignition (HCCI) engine operation offers the potential to provide fuel economy approaching that of traditional diesel engines, with increased compression ratios and low pumping losses, while simultaneously emitting low NO_x and soot due to the homogeneous, low temperature nature of the combustion. HCCI, however, comes with unique challenges as fuel mixture chemical kinetics supplant direct ignition timing control via spark ignition or injection timing. Improved understanding of the ignition phenomena that control in-cylinder combustion phasing and duration in HCCI engines can help overcome the challenges of HCCI. In particular, spark-assisted HCCI combustion has been proposed as a means to extend HCCI operating limits and to facilitate transition between spark-ignition and HCCI operating modes.

The current work presents the results of an experimental study characterizing the ignition phenomena observed during HCCI lean operating conditions using high-speed digital imaging and the optical access provided by a single-cylinder optical

research engine. Three fuels (indolene, iso-octane, and pump gasoline) and a range of operating conditions, including spark-assisted HCCI operation, were examined. HCCI combustion was initiated and maintained over a range of lean conditions, from equivalence ratios of $\phi = 0.69$ to 0.27. Time-resolved imaging and pressure data showed high rates of heat release in HCCI combustion correlated temporally to rapid volumetric ignition occurring throughout the combustion chamber. Lower rates of heat release were characteristic of spatially-resolved ignition and subsequent propagation of reaction fronts. Gasoline and indolene exhibited similar HCCI imaging characteristics and in-cylinder pressure time-histories, while iso-octane showed a dramatic transition into misfire. Preferential ignition sites within the combustion chamber were identified based on the imaging and were considered clear markers of thermal stratification. The results for iso-octane indicate misfire at low load has distinctly different ignition characteristics (with well resolved, localized ignition and propagation) compared to stable HCCI (with volumetric ignition).

The results of the spark-assisted HCCI study demonstrated that spark assist stabilized HCCI combustion and extended lean operating limits for a window of engine operating conditions. The imaging data showed two ignition regimes exist. One regime is typified by an initial local reaction zone formed around the spark plug, which accelerates subsequent compression ignition sites that consume the fuel charge. The second regime is typified by consumption of the fuel charge by radial reaction front propagation from the spark plug. Regions of high sensitivity of HCCI operation to spark assist were bounded by low and high air preheat conditions. Within the temperature bounds, the effectiveness of spark-assisted HCCI was a strong function of the equivalence ratio and spark timing. Spark assist clearly extended low load HCCI operation within acceptable engine operating metrics, such as rate of pressure

rise and indicated mean effective pressure.

CHAPTER I

Introduction

Ignition and combustion are the most important processes in homogeneous charge compression ignition (HCCI) engines, and these phenomena are considered limited by chemical kinetics. HCCI engines have several potential advantages over traditional spark ignition (SI) and diesel engines [5, 6]. HCCI offers greater fuel economy than SI engines, because they are capable of higher compression ratios and reduced throttling losses. HCCI engines also offer lower NO_x and particulate emissions than diesel engines, as a result of reduced local high-temperature zones and the homogeneous nature of the reaction. HCCI engines, however, present unique challenges, as chemical kinetics supplant traditional control strategies (i.e. spark ignition and diesel injection timing).

Recent rapid compression facility (RCF) studies of iso-octane/air mixtures by He et al. [7] and Walton et al. [8, 9, 10] have demonstrated the presence of distinct ignition regimes. Under low fuel mole fraction conditions, only volumetric ignition was observed [7, 8]. At higher fuel mole fractions, reaction fronts appeared to propagate throughout the test chamber of the RCF prior to volumetric ignition [8]. The presence of the reaction fronts served to accelerate ignition. The presence of similar phenomena during HCCI operation of a reciprocating piston engine could compli-

cate ignition timing and the development of robust timing strategies. Additionally, Kaiser et al. [11, 12] observed a dramatic change in the engine-out emissions at equivalence ratios of approximately 0.2 in their study of a single-cylinder engine operating in HCCI mode using gasoline fuel. Kaiser et al. [12] proposed that the shift in emissions could be explained by flame propagation over relatively short distances for equivalence ratios less than 0.2. The debate over the presence of reaction fronts motivates in part this research study.

The objective of the first part of the research program was to characterize the ignition phenomena observed during HCCI lean operating conditions for three classes of fuels: a reference fuel (indolene), a commercial fuel (pump gasoline) and a chemical surrogate fuel (iso-octane). Iso-octane is often used as a chemical surrogate for gasoline, and indolene is used as a reference grade fuel for gasoline. Thus, differences in the fuel performance and relationships to ignition phenomena provide insight into translating trends in prototype engine studies to production engines. Such characterization is also necessary to establish a baseline for understanding differences in weak and strong HCCI operation and how these conditions are related to changes in ignition and combustion behavior.

The most significant challenge of homogeneous charge compression ignition (HCCI) engines is the development of control strategies that allow effective HCCI operation over the largest possible operating regime of the engine. Extending the operating limits of HCCI is critical to realize the considerable efficiency and emissions benefits that are the hallmark of HCCI. Researchers are exploring several approaches including spark-assist [3, 13, 14, 15, 16, 17, 18], variable valve timing [3, 19] and variable compression ratio [20, 21, 14] methods to achieve the goal of improved HCCI performance.

Of these methods, many show promise, particularly spark-assisted HCCI. The use of spark-assist as a control method for HCCI operation has been studied in various aspects. One subset of research considers strategies to enable transitions from/to spark ignition (SI) and HCCI operation [17, 3, 14]. Other researchers have concentrated on initiating ignition of a globally lean charge with spark ignition of a locally rich stratified zone in a direct injection engine [15, 22]. Another broader subset of research considers the use of spark-assisted HCCI to extend the range of low temperature combustion (LTC) operation[16, 13, 14]. All of these research efforts, however, lack fundamental insight into the nature of the spark-assisted ignition event and how it influences further bulk ignition. One study by Weinrotter et al. [13] did investigate optical diagnostics of laser-induced and spark-plug assisted HCCI combustion. That study attempted to explain how and to what extent the spark influences the auto-ignition process or whether primarily normal compression-ignition induced ignition prevails; the study, however, was inconclusive. All of the spark-assisted HCCI studies have also shown some variability on the magnitude of the effect of spark-assist. For example, spark-assist did not affect heat release during combustion in the HCCI studies by Weinrotter et al. [13], although imaging showed differences in the ignition systems considered. The objective of the secondary area of the dissertation research program was to understand the effects of spark-assist on ignition with a particular focus on low load/lean operation. The fundamental hypothesis of this aspect of the work was that spark-assist can be used to extend HCCI operation over a large range of load and engine speed conditions and that optical imaging can dramatically accelerate the understanding necessary to advance these methods. To understand the effects of spark-assist on the physical and chemical mechanisms important during spark-assisted HCCI, the lean operating limits were

quantified while simultaneously using high-speed imaging to monitor the in-cylinder ignition and combustion phenomena.

The following chapters describe the results of the series of experimental optical engine studies. Chapter II presents a detailed description of the new University of Michigan optical engine facility created to conduct these studies. Chapter III presents the operating conditions and results of the multiple fuel studies. Chapter III includes a discussion of the results and conclusions based on this part of the study. Chapter IV presents the operating conditions and results of the spark-assisted HCCI studies. Chapter IV includes results of multi-axis imaging (through the piston window insert and through a transparent cylinder liner), imaging results from the parametric study conducted over a large range of engine operating conditions, and results for engine performance metrics. Conclusions based on the spark-assisted study are included in Chapter IV. Chapter V presents the conclusions and future work based on the overall HCCI optical engine imaging research program.

CHAPTER II

Optical Research Engine Facility

The primary objective of the new optical research engine facility at the University of Michigan (UM) is to provide improved understanding of the chemical and physical mechanisms that are important in advanced engine systems, including expanded HCCI and other low- temperature combustion strategies. Research conducted with the optical engine research facility complements that conducted using the UM RCF, expanding to experiments with multiple cycles in a flexible, production-based engine configuration. In the following sections, the optical engine facility used to conduct the studies is presented.

2.1 Optical Research Engine

All experiments were conducted using the new UM single-cylinder optical research engine facility. This facility is based on an optical research engine donated to the UM by the Ford Motor Company. The optical research engine design is conceptually based on the optical research engine developed by Sandia National Laboratories [23]. The facility features a hydraulically-supported, drop-down cylinder liner assembly with interchangeable fused silica and steel cylinder liners supporting a Bowditch-style piston extension with a quick-release top piston. The piston features a removable

crown insert window, made of either fused silica or aluminum. An elliptical mirror is fixed in the piston extension for optical access through the ∅48.5 mm piston window. The resulting facility offers excellent axial and orthogonal optical access through the piston window/mirror and the cylinder liner (Fig. 2.1).

The optical research engine, depicted in Figure 2.2, is built around a Ford Zetec-SE 1.25 L engine configuration. This engine was originally built in Valencia, Spain for the 1997 Ford Fiesta (European). A modified production cylinder head is used, employing one of the four cylinders available. The aluminum cylinder head features fixed double-overhead cams (Fig. 2.2) timing 4 valves (twin ∅26.1 mm intake, twin ∅22.1 mm exhaust) around a centrally mounted spark plug (Fig. 2.3). A flat-top ∅71.9 mm piston with Torlon® rings strokes 76.5 mm for 0.31 L displacement at 10:1 compression ratio. Fuel is port injected slightly upstream of the twin intake ports. More details regarding the optical research engine and its components are included in Appendix A.

The engine is driven by an Electro-Mechanical Associates Micro-Dyn 35 hydraulic dynamometer (built jointly with UM). Typical experiments held the engine speed constant at 700 RPM. The hydraulic dynamometer has an automatic control system to maintain set speed by compensating between providing a motoring load and absorbing net power output. Engine coolant and oil are auxiliary heated; coolant was maintained at 90 °C and oil was maintained at 60 °C. The engine was typically pre-conditioned by circulating heated coolant for at least 45 minutes. The engine was then motored by the dynamometer for another 30 minutes to stabilize oil temperature and intake air conditions before running experiments. More details regarding the dynamometer, lubrication, and cooling systems are included in Appendix B.

Fuel was fed to the Siemens DEKA II center-feed dual conical jet injector at 1.7

atm. A Magnatek Engine Control Module (ECM) spark and fuel injection controller is integrated with the dynamometer. Fuel equivalence ratio was controlled by varying the fuel injector driver pulse width duration, holding fuel rail pressure constant. More details regarding the fuel handling, fuel injector controller, and ignition systems are included in Appendix B.

All experiments in this study were run with the same near Wide-Open-Throttle (WOT) throttle plate setting, with the fuel injection pulse width varied to control the overall equivalence ratio of the fuel/air mixture. While this caused various equivalence ratios to have different engine loadings, the fixed throttle plate setting allowed fewer changes to the engine operating conditions to achieve HCCI for various equivalence ratios.

Figure 2.4 presents the exhaust and intake valve timing used for all experiments. Fuel was injected very early onto a closed intake valve, at 50° Before-Top-Dead-Center (BTDC) during the compression stroke of the preceding cycle, to assist fuel vaporization (and help cool the exhaust valves). Ambient air was preheated with a 1.4 kW heater and the intake manifold was heated using an auxiliary resistive heater to deliver various intake air temperatures of approximately 250-320 °C just upstream of the fuel injector. Note, the thermocouple measurement at this location is not the cylinder charge temperature. Several processes (e.g. fuel vaporization) affect the air temperature, which are discussed further in Chapter III. More details regarding the intake, exhaust, and crankcase ventilation systems are included in Appendix B.

2.2 High Speed Imaging

The combustion chamber was imaged through the piston window using a high-speed color digital video camera (Vision Research Phantom v7.1, color). The camera is capable of 800 x 600 pixel spatial resolution, and reduced resolution frame rates up to 160 kHz. A fast 50 mm lens (f/0.95 Nikor TV lens) and C-mount extension tubes are used with the camera to adjust the focal length and to reduce the focal depth along the cylinder axis. In this study, the camera was focused at a plane coinciding with the spark plug ground electrode. The camera settings were generally fixed at 320 x 320 pixels for piston window imaging (or 640 pixels wide x 480 pixels high for orthogonal cylinder liner imaging) at 3000 frames per second (fps) with 309 μs exposure time. The camera sensor array was calibrated according to the procedure outlined in Walton et al. [9]. Fig. 2.5 depicts the orientation of the imaged frames and the engine valve geometry. The piston window is ∅48.5mm, which partially occludes the valves. Recall the piston diameter is ∅71.9 mm. Thus, 45.5% of the cylinder is imaged. More details regarding the camera imaging system are included in Appendix C.

Non-filtered, visible chemiluminescence emission was recorded via the high-speed color digital camera and time-sequenced with crank-angle resolved pressure data. Camera images were time sequenced to a common trigger with other data, and were color and gain adjusted to improve image viewing clarity. All time-recorded data were then transcribed into crank-angle basis with respect to compression stroke Top-Dead-Center (TDC).

For the visible spectra of interest (violet at approximately 400-450 nm through blue at approximately 450-495 nm through green at approximately 495-570 nm),

Figure 2.6 shows the Vision Research v7.1 camera has a quantum efficiency between 20-35% [1]. Figure 2.7 shows the spectral response for each of the three color channels, indicating the relative light transmission through the red, green, and blue color filters as a function of incoming light wavelength [1]. The blue channel is centered around approximately 460 nm, with transmission sharply falling below approximately 400 and above 500 nm. The green channel is centered around 550 nm, with transmission sharply falling below approximately 475 and above 580 nm. The chemiluminescence emission captured by the camera was not additionally filtered by wavelength beyond the inherent camera, lens, and in-cylinder window response characteristics.

Figure 2.8 is a typical combustion reaction front image captured with the high-speed imaging system for a typical indolene experiment. The image shows clear spatial definition to the blue chemiluminescence emission. The visible blue emission recorded by the camera is attributed to C_2, CH, or possibly CO. C_2 and CH each have strong emission bands in the blue spectral region (C_2: 473.7 nm, 516.5 nm, 563.5 nm; CH: 431.2 nm [24, 25]). C_2 and CH are short-lived intermediate species, and are considered good indicators of high temperature reaction zones. CH has been used in numerous flame studies as a marker of the flame zone (e.g. [26, 27]). CO is a longer lived combustion species with an emission band located broadly around 380 nm [24, 25]. Based on the camera spectral response properties presented above, the blue emission is not likely due to CO. Consequently, the blue emission observed in these experiments is considered indicative of high-temperature regions of high rates of reaction.

2.3 Instrumentation and Data Acquisition

Cylinder pressure is measured using a piezoelectric transducer (Kistler 6125A) and charge amplifier (Kistler 5010B). Intake pressure is measured with an absolute pressure sensor in a water cooled fitting (Kistler 4045A2 with Kistler 4618 amplifier). The water cooled fitting is necessary for the intake pressure sensor to protect it against high intake temperatures. Pressure data were not filtered prior to recording. More details regarding the pressure transducers are included in Appendix C.

Crank angle is encoded with a BEI encoder at 360 signal cycles per revolution, with a secondary channel output signaling TDC. In addition to the aforementioned intake manifold thermocouple, other thermocouples record coolant temperature leaving the cylinder head, and oil temperature entering the engine. More details regarding the crank angle encoder and thermometry are included in Appendix C.

Equivalence ratio is measured in the exhaust manifold using an ETAS LA4 lambda meter utilizing a Bosch broadband LSU 4.9 lambda sensor. The lambda meter calculates equivalence ratio based on the O_2 content of the exhaust stream, given the following inputs:

- fuel H/C ratio
- fuel O/C ratio
- fuel H_2O component
- stoichiometric air / fuel mass ratio

Since the lambda meter falsely reads excess exhaust O_2 due to incomplete combustion and misfire as a mixture leaner than actual, some procedural development was required. For each intake temperature, a series of experiments were conducted to map out the relationship between fuel pulse width and the ETAS LA4 lambda

meter's interpretation of equivalence ratio. For lean mixtures which resulted in incomplete combustion in HCCI mode, advanced spark ignition was used to provide more complete combustion in these trials. The equivalence ratio for that more complete combustion condition was then used as a reference for that particular fuel pulse width / intake temperature combination. This procedure helped correct readings for most lean mixtures. Corrections for very lean conditions were estimated by interpolation from other conditions. More details regarding the ETAS LA4 lambda meter are included in Appendix C.

Data acquisition was performed using a National Instruments Compact Data Acquisition (cDAQ). This Universal Serial Bus based system recorded temperature readings at the beginning of each experiment, then recorded all digital and analog channels at 100 kHz, using a LabView software code. More details regarding the cDAQ system and LabView code are included in Appendix C.

MATLAB codes were written for processing time-based crank angle encoder and pressure data. These codes are included in Appendix D. Later experiments used smoothing of pressure data to allow better derivative based calculations (including apparent heat release), as documented in Appendix C. Cylinder pressure transducer measurements were also corrected from relative measurements to absolute measurements (commonly known as "pegging") via MATLAB post-processing. The method used was to reference the cylinder pressure transducer to the intake manifold transducer at Bottom-Dead-Center (BDC) of the intake stroke [28, 29]. The software for the Vision Research digital camera was used to synchronize time-based imaging data to the processed crank angle encoder and pressure data.

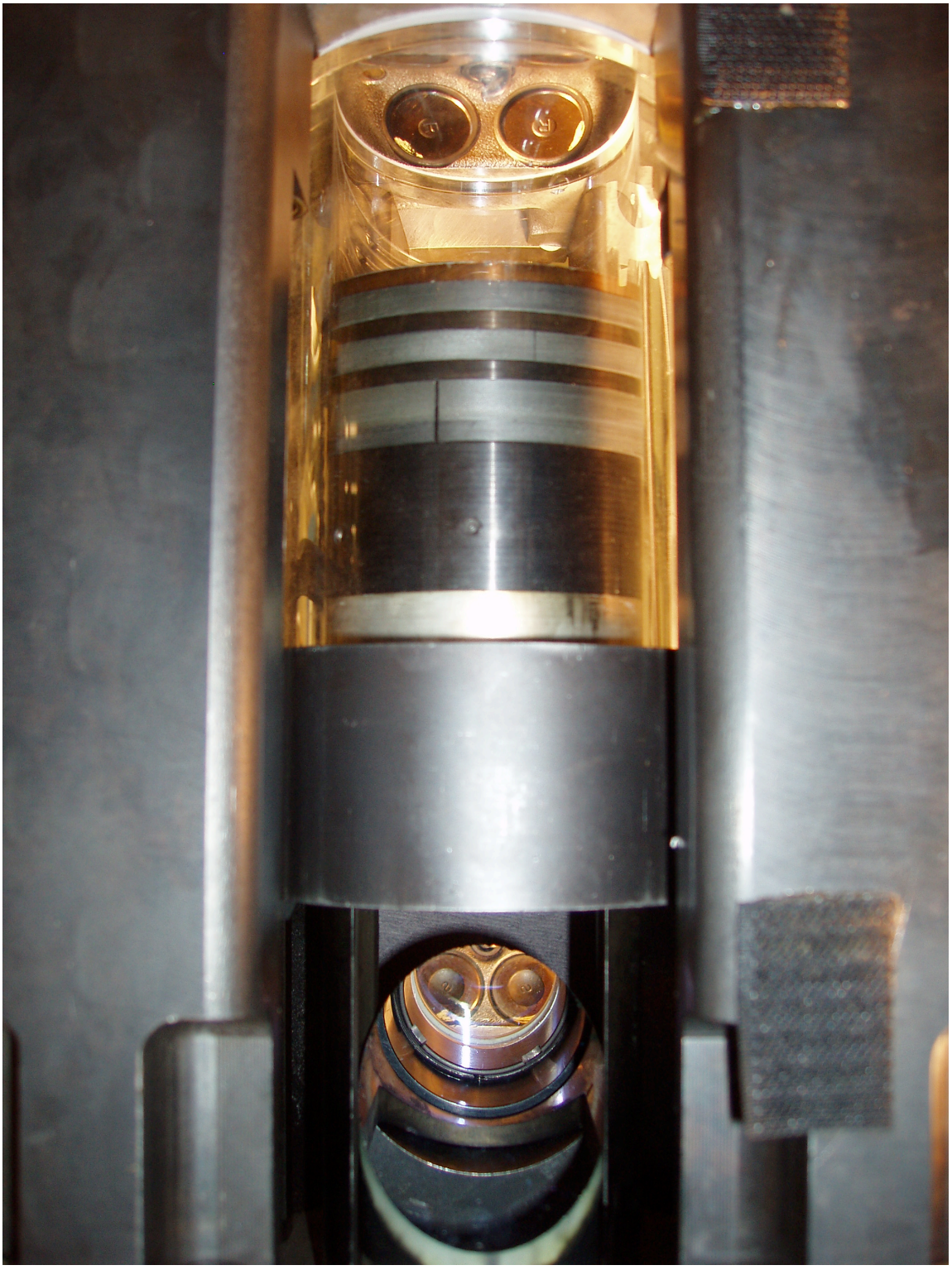

Figure 2.1: View of the single cylinder optical research engine showing the full fused silica cylinder liner and piston assembly at the top.

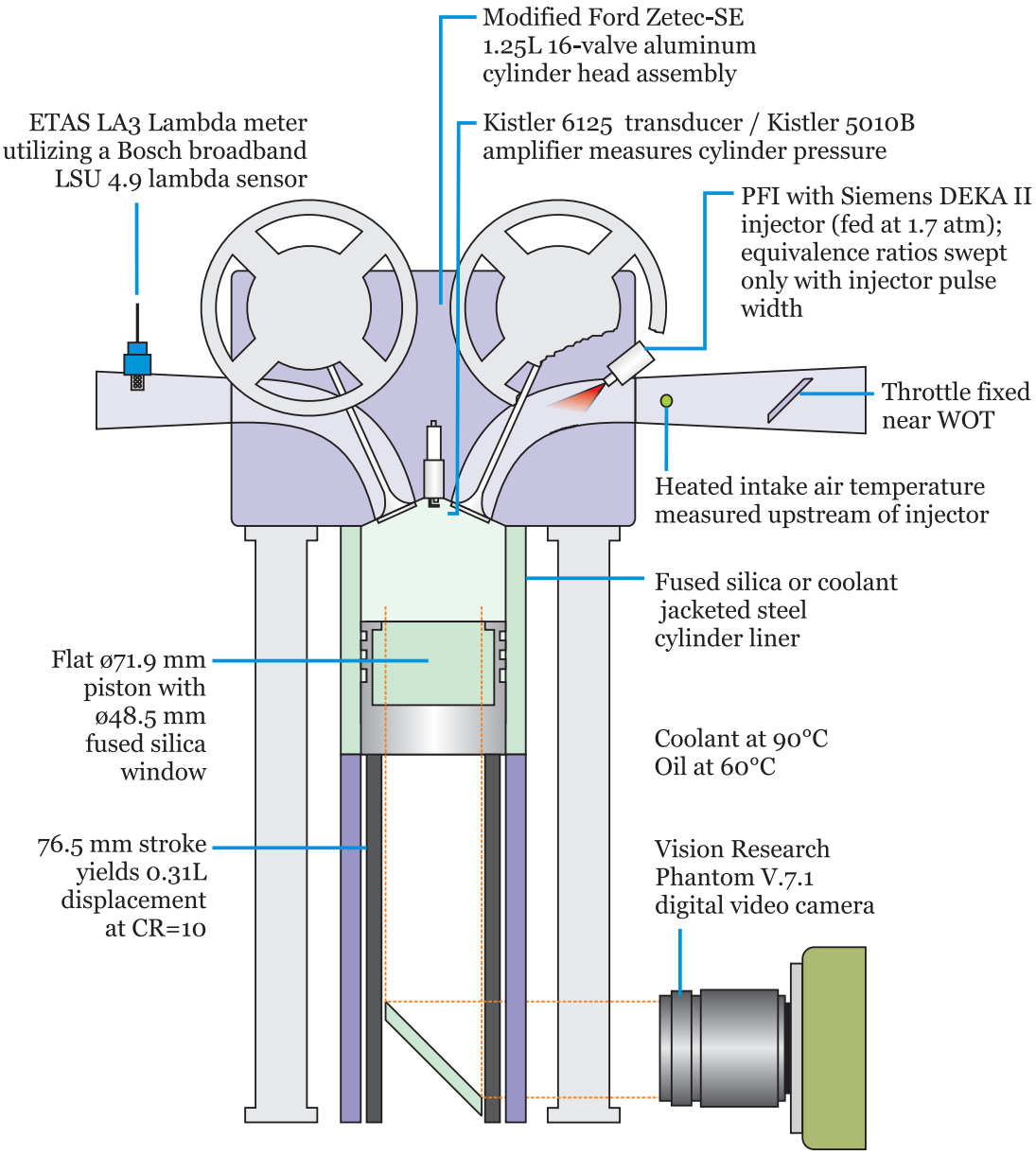

Figure 2.2: Schematic of the single-cylinder optical research engine.

Figure 2.3: View of the intake valves (top), exhaust valves (bottom), and centrally mounted spark plug, as viewed through the mirror and piston window.

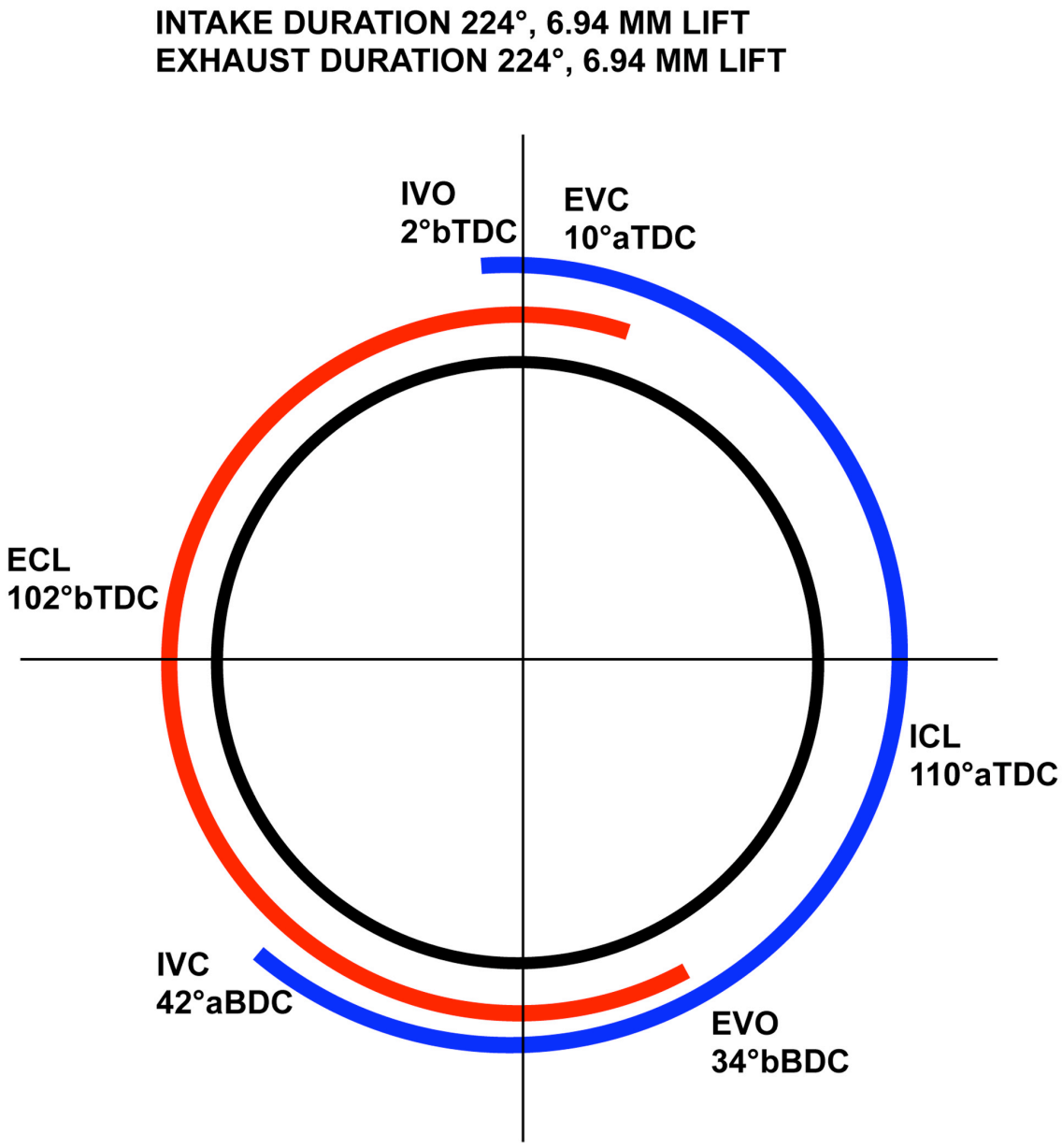

Figure 2.4: 1.25L engine intake and exhaust cam timing events.

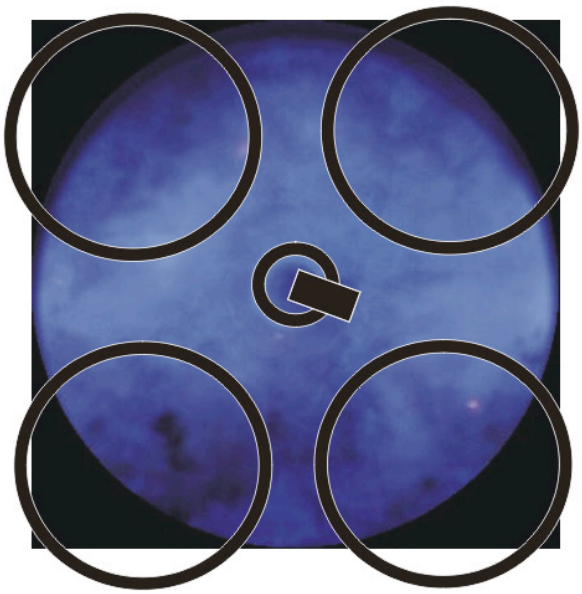

Figure 2.5: Orientation of the imaged frames with respect to the cylinder geometry. Intake valves are on the bottom, and exhaust valves on the top. The spark plug is shown at the center.

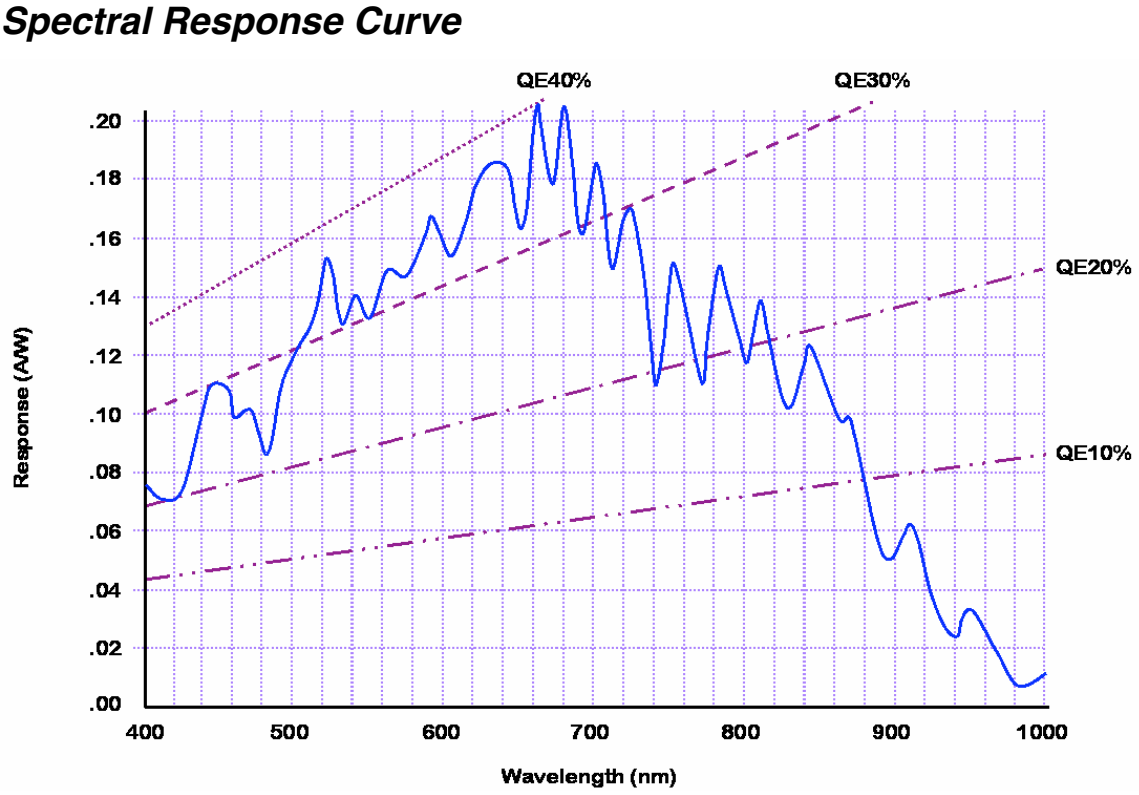

Figure 2.6: Spectral response curve of the Vision Research v7.1 camera, indicating signal current output from the sensor array for an incoming light beam of a given power and wavelength [1]. Responsivity in amperes output per watt light input is displayed as a function of incoming light wavelength. The plot also displays lines of quantum efficiency, percentage of photons hitting the photoreactive surface that will produce a signal.

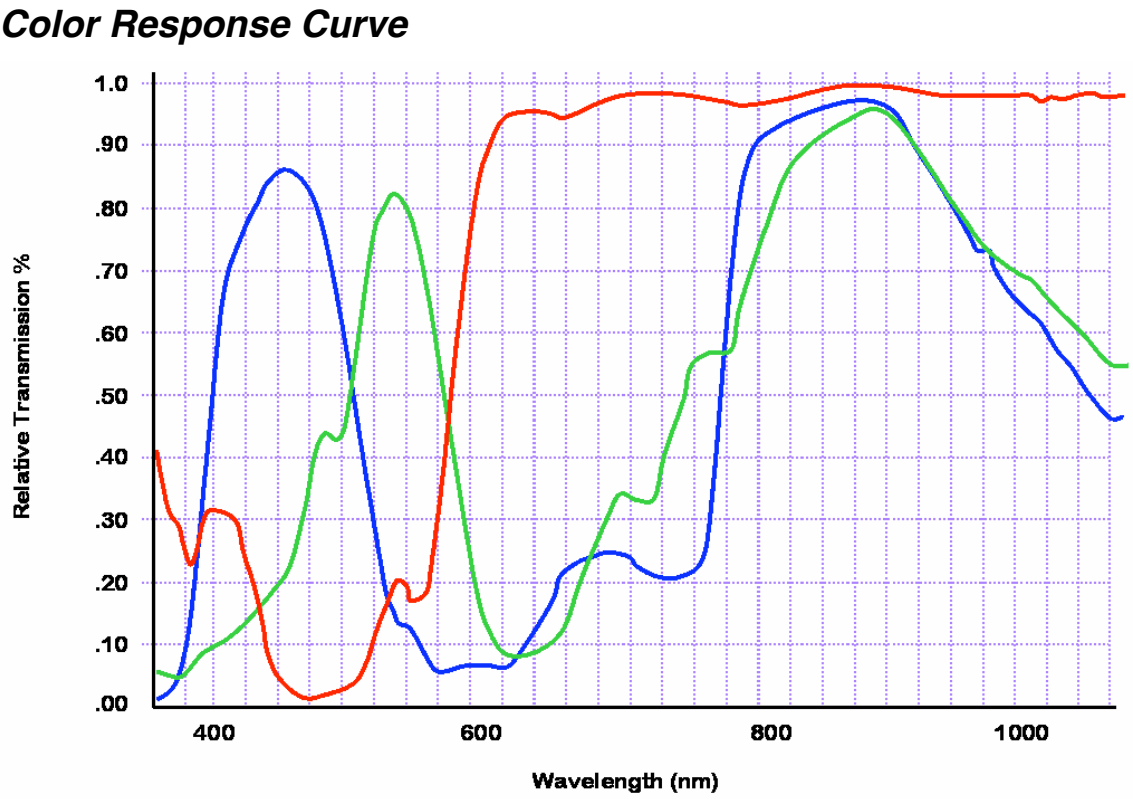

Figure 2.7: Color response curve of the Vision Research v7.1 camera, indicating relative light transmission through the red, green, and blue color filters separating the color channels, as a function of incoming light wavelength [1].

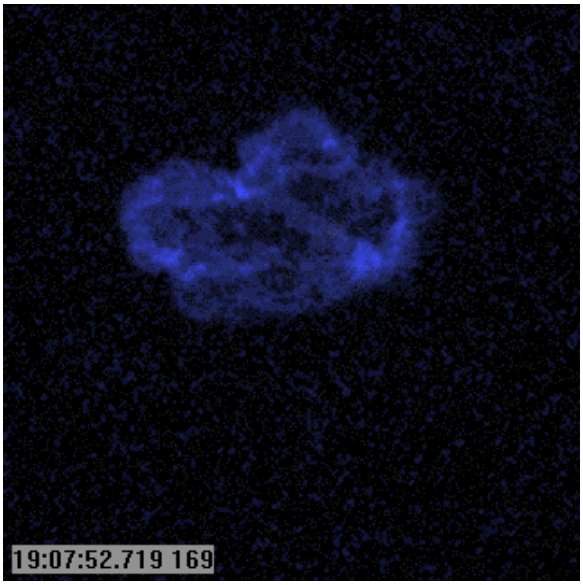

Figure 2.8: Single image of a combustion reaction front as captured by the high speed imaging system through the piston window for an indolene experiment. The image, which has been gain adjusted for viewing clarity, provides spatial definition of blue chemiluminescence emission, which are indicative of high temperature reaction zones.

CHAPTER III

HCCI Ignition Study of Multiple Fuels

3.1 Introduction

The objective of this part of the research program was to characterize the ignition phenomena observed during HCCI lean operating conditions for three classes of fuels: a reference fuel (indolene), a pump fuel (pump gasoline) and a chemical surrogate fuel (iso-octane). Iso-octane is often used as a chemical surrogate for gasoline, and indolene is used as a reference grade fuel for gasoline. Thus, differences in the fuel performance and relationships to ignition phenomena provide insight into translating trends in prototype engine studies to production engines.

High speed imaging combined with the optical access provided by the research engine offered the ability to directly image and compare ignition and combustion phenomena for the fuels considered. Lean operating limits were the focus of the study with the primary objective of identifying different modes of reaction front initiation and propagation for each fuel.

Most of the material in this chapter has been published in the ASME Journal of Engineering for Gas Turbines and Power [30].

3.2 Experimental Approach

For each experiment, the intake air was preheated as well as the engine coolant and oil. The engine was motored until a steady condition was reached. Intake air preheating was required to achieve HCCI combustion. Once the engine speed was stabilized by the dynamometer and preheated air was introduced to the cylinder, HCCI combustion was initiated with fuel delivery only; no ignition spark was used to initiate firing and then transition to HCCI. The engine was operated through a range of lean conditions as listed in Table 3.1. The fuels used in this work included iso-octane (2,2,4 tri-methyl pentane; Sigma-Aldrich, anhydrous 99.8%), indolene (analyzed at 87.12% by weight carbon, <0.05% oxygen, 12.88% hydrogen; H/C = 1.762; 97.4 RON, 88.3 MON, 92.9 AKI), and commercial gasoline (Shell V-Power 93 octane (AKI) summer blend, assumed H/C = 1.85 for lambda meter programming). Properties for two additional fuels used for modeling predictions, reference gasolines 1 and 2, were obtained from [31]. Reference information for the Shell commercial gasoline was estimated from the U.S. Code of Federal Regulations for U.S. Environmental Protection Agency regulatory calculations [32]. A summary of this information is found in Table 3.2.

3.3 Results

3.3.1 Indolene

Examples of typical pressure traces for each indolene equivalence ratio condition are shown in Fig. 3.1. The image sequences shown in Figures 3.2 - 3.5 correlate to each of the pressure traces, as indicated by equivalence ratio in Fig. 3.1. The pressure

Table 3.1: Experimental engine operating conditions studied in HCCI mode for each fuel.

Fuel	ϕ	Intake Air Temperature (°C)
Indolene	0.69	317
Indolene	0.55	317
Indolene	0.44	317
Indolene	0.34	318
Iso-octane	0.68	319
Iso-octane	0.61	319
Iso-octane	0.45	319
Iso-octane	0.29	318
Gasoline	0.65	316
Gasoline	0.52	318
Gasoline	0.45	316
Gasoline	0.37	317
Gasoline	0.27	316

traces for $\phi = 0.69$ and $\phi = 0.55$ showed little cycle-to-cycle variation; however, leaner conditions exhibited considerable irregularity. Pressure traces at conditions of $\phi = 0.69$ and 0.55 show ignition during compression and high heat release rates. Pressure traces at $\phi = 0.44$ showed ignition closer to TDC, with lower rates of heat release. For $\phi = 0.34$, the pressure traces show HCCI combustion began during the expansion stroke, occurring later with leaner conditions.

Figures 3.2 - 3.5 show image sequences for HCCI combustion of indolene at various equivalence ratios. Each imaging frame represents a time interval of 333 μs, which at 700 RPM translates to 1.4 crank angle degrees (CAD). The time markers shown in the imaging frames are with respect to an arbitrary camera synchronization trigger signal for each experiment. All images have been gain adjusted for clarity.

Each of the series show blue emission originating in a localized area in the combustion chamber. The time observed for the blue emission to expand from the point of origin to the remainder of the combustion chamber increased with leaner conditions. At $\phi = 0.69$, relatively uniform blue emission consistently developed across the combustion chamber within one image sequence (1.4 CAD) of the first indication

Table 3.2: Fuel properties used in modeling and experiments.

Fuel	Formula	Stoich. O_2 Coeff.	Mass $(A/F)_s$	H/C	Heat of Vaporization [kJ/kg]	LHV [MJ/kg]	RON	MON	(R+M)/2
Iso-octane	C_8H_{18}	12.5	15.10	2.25	308	44.3	100	100	100
Ref. Gasoline 1 [31]	$C_{8.26}H_{15.5}$	12.135	14.57	1.877	350	44	91-99	82-89	N/A
Ref. Gasoline 2 [31]	$C_{7.76}H_{13.1}$	11.035	14.30	1.688	N/A	44	N/A	N/A	N/A
Indolene	$C_{7.25}H_{12.78}$	10.448	14.41	1.762	N/A	43.3	97.4	88.3	92.9
Gasoline (Shell) [32]	$C_7H_{12.95}$	10.238	14.53	1.85		N/A	N/A	N/A	93

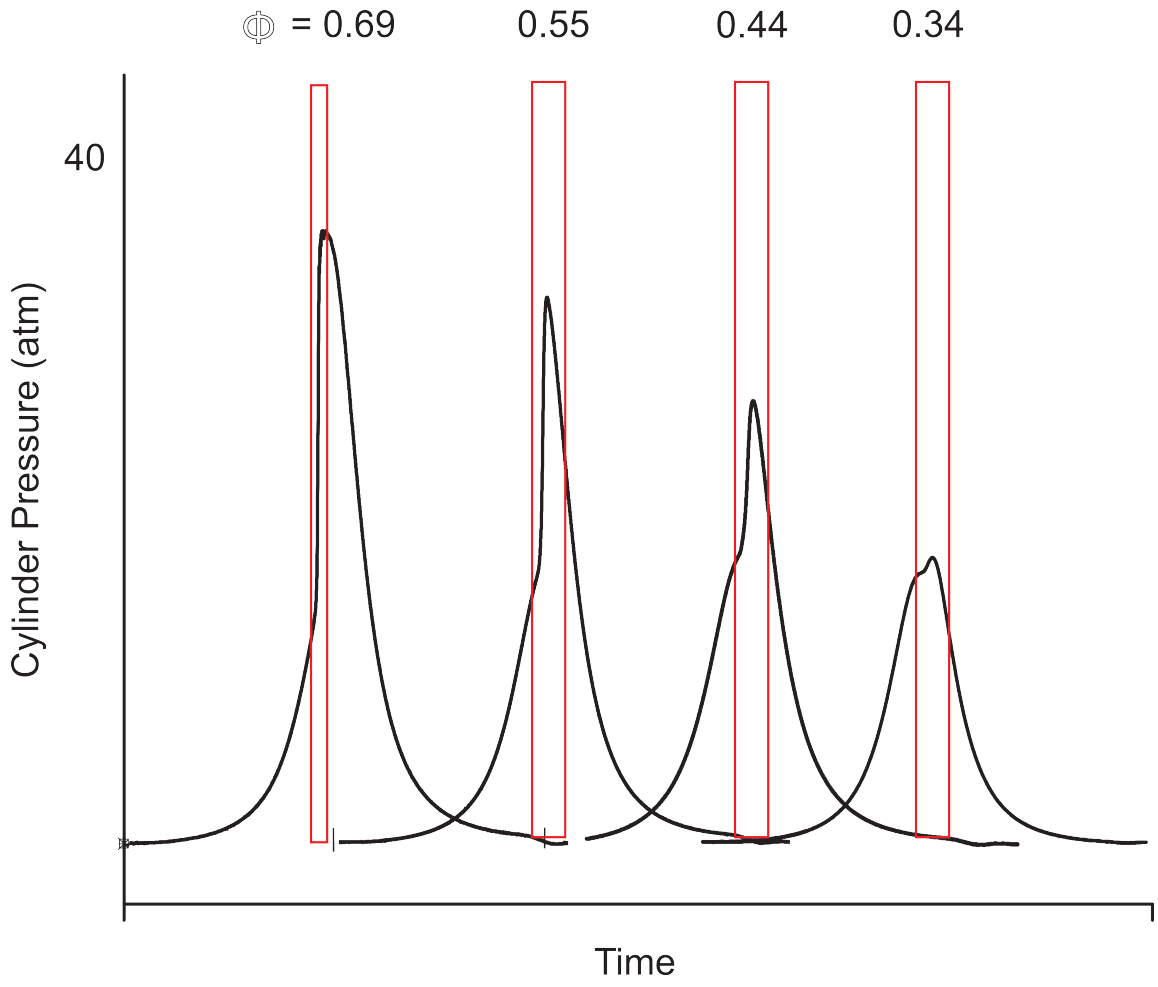

Figure 3.1: Typical pressure time histories for engine conditions with indolene fuel. The data are superimposed for clarity. The boxed areas coincide with the imaging sequences shown in Figures 3.2 - 3.5.

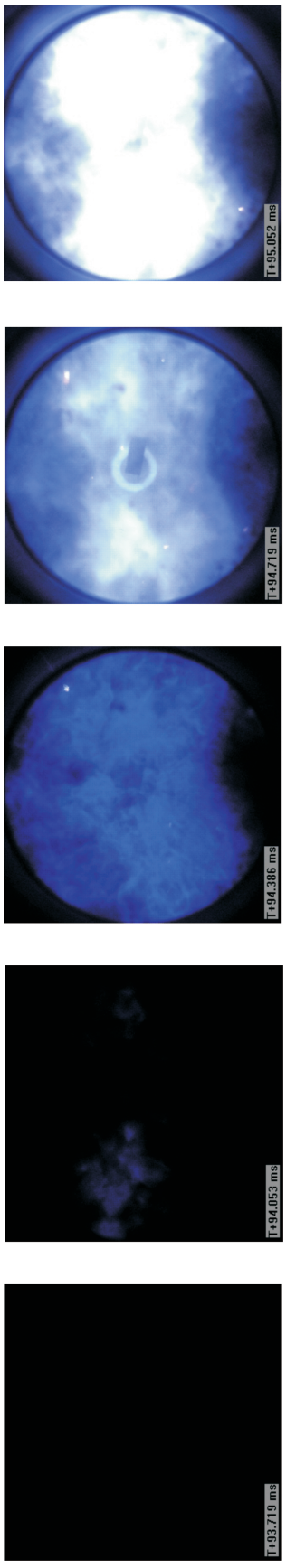

Figure 3.2: Image sequence for indolene at $\phi = 0.69$.

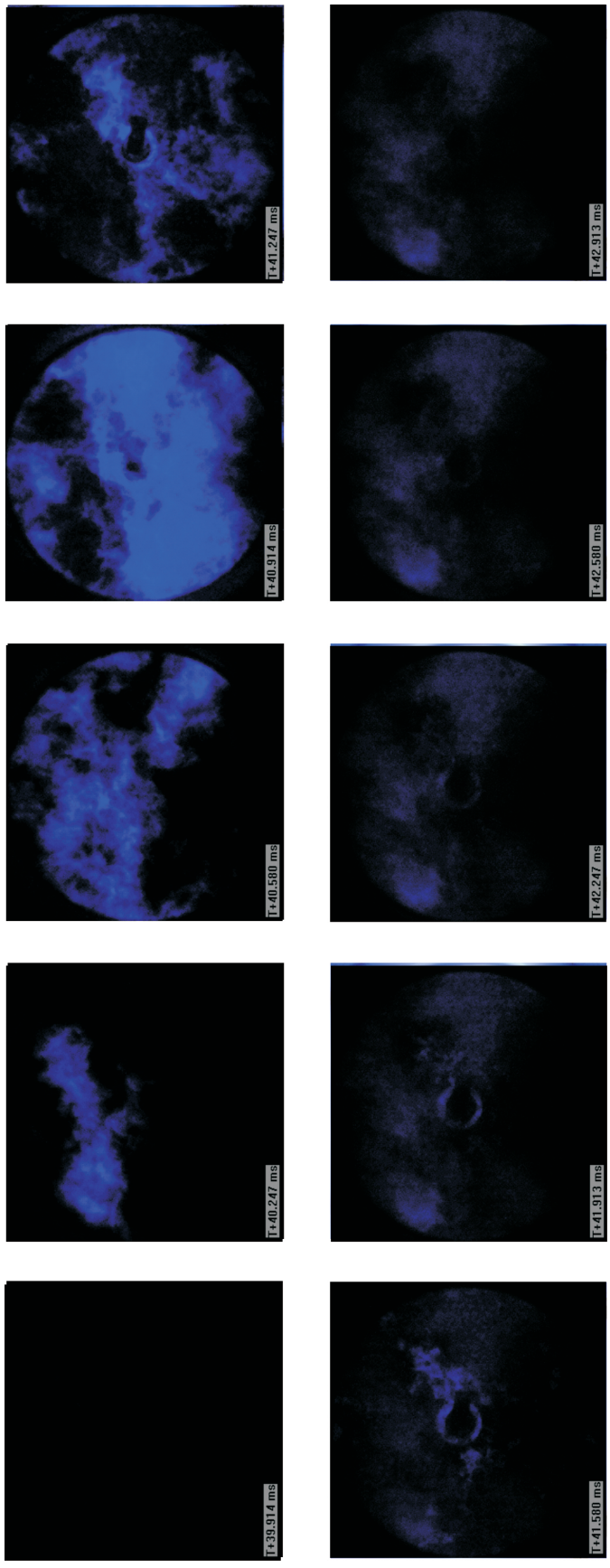

Figure 3.3: Image sequence for indolene at $\phi = 0.55$.

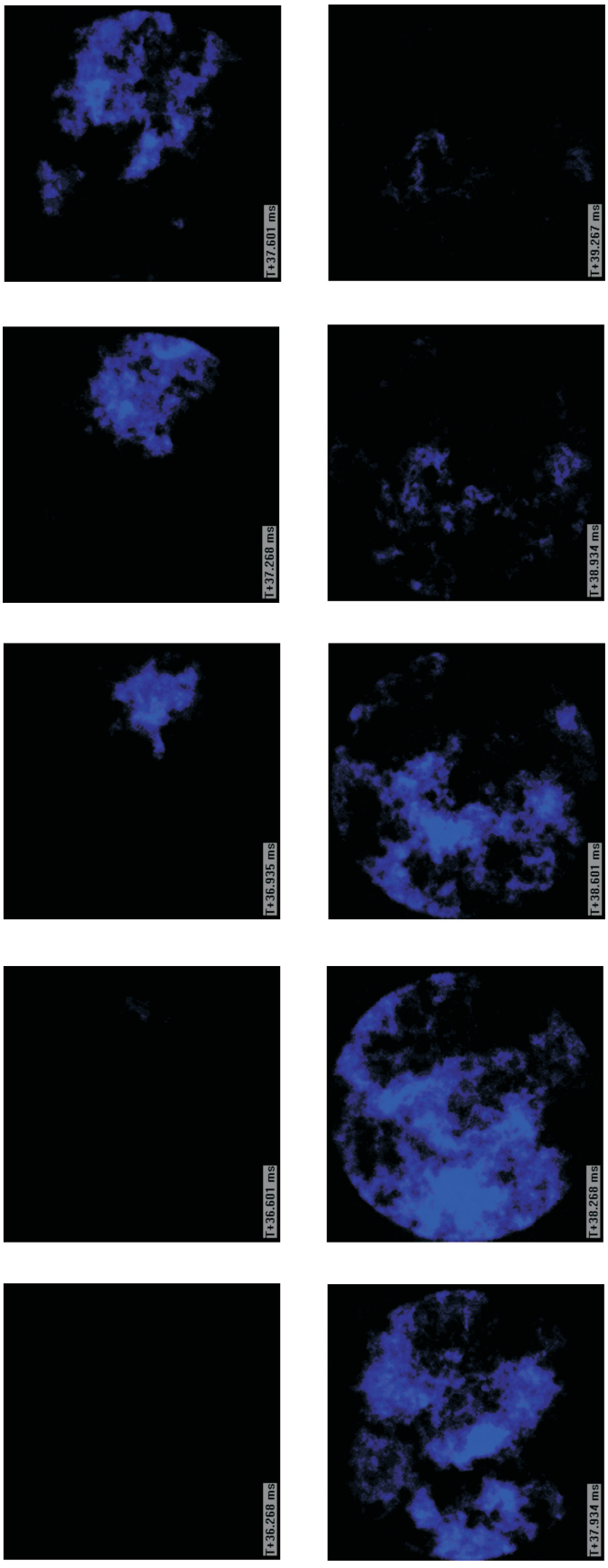

Figure 3.4: Image sequence for indolene at $\phi = 0.44$.

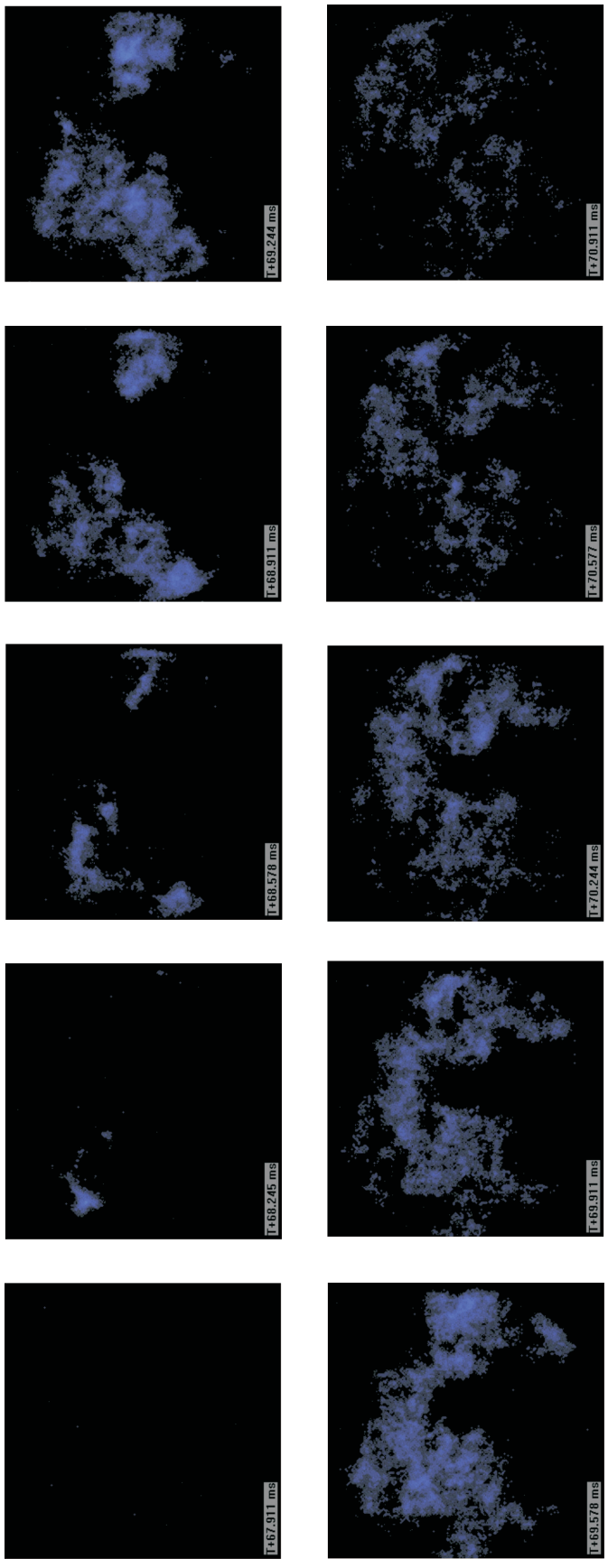

Figure 3.5: Image sequence for indolene at $\phi = 0.34$.

of ignition. The data at $\phi = 0.55$ showed similar, but slightly longer time to observe emission throughout the cylinder. At leaner conditions, the propagation required significantly longer times and emission never appeared simultaneously throughout the volume of the combustion chamber.

The images obtained at $\phi = 0.69$ (Fig. 3.2) showed bright white emission, which could be attributed to saturation of the camera array or thermal emission from soot particles. Further experiments, discussed below, indicate the white emission is due to camera pixel saturation. Leaner conditions did not produce white emission.

The rapid heat release rates characterized as rapid increases in the pressure data for $\phi = 0.69$ and 0.55 in Fig. 3.1 correspond temporally to the visualization of intense blue emission throughout the volume of the combustion chamber as seen in the imaging sequences of Figures 3.2 and 3.3. The less pronounced heat release rate seen in Fig. 3.1 for $\phi = 0.44$ corresponds to emission occupying slightly less than the complete volume and less intense blue emission, as seen in Fig. 3.4. The spatially resolved, weaker blue emission seen in Fig. 3.5 for $\phi = 0.34$ corresponds to the small pressure rise on the expansion stroke seen in Fig. 3.1.

3.3.2 Iso-Octane

Examples of typical pressure traces for each iso-octane run are shown in Fig. 3.6. The image sequences shown in Figs. 3.7 - 3.10 correlate to the pressure traces where indicated in Fig. 3.6, with the exception of the image sequence for $\phi = 0.45$ (see Figure 3.9). The imaging sequence for that experiment was not synchronized with pressure data. Consequently, a typical but not matching sequence of images is presented for that condition.

The cylinder pressure traces for $\phi = 0.68$ showed ignition during compression,

high heat release rates, and little cycle-to-cycle variation. Sequential pressure traces for $\phi = 0.61$ showed considerable variation, indicating misfire instability. The misfire conditions showed variation including ignition during compression, ignition during the expansion stroke, and pressure data resembling motoring conditions. Fig. 3.6 contains an example of one of the most prevalent firing cycle behavior modes for $\phi = 0.61$. The leaner $\phi = 0.45$ and 0.29 conditions showed much less cycle-to-cycle variation in the pressure profiles; however, the peak pressures were very low, resembling motoring pressure data. There was little obvious ignition-induced effect on pressure.

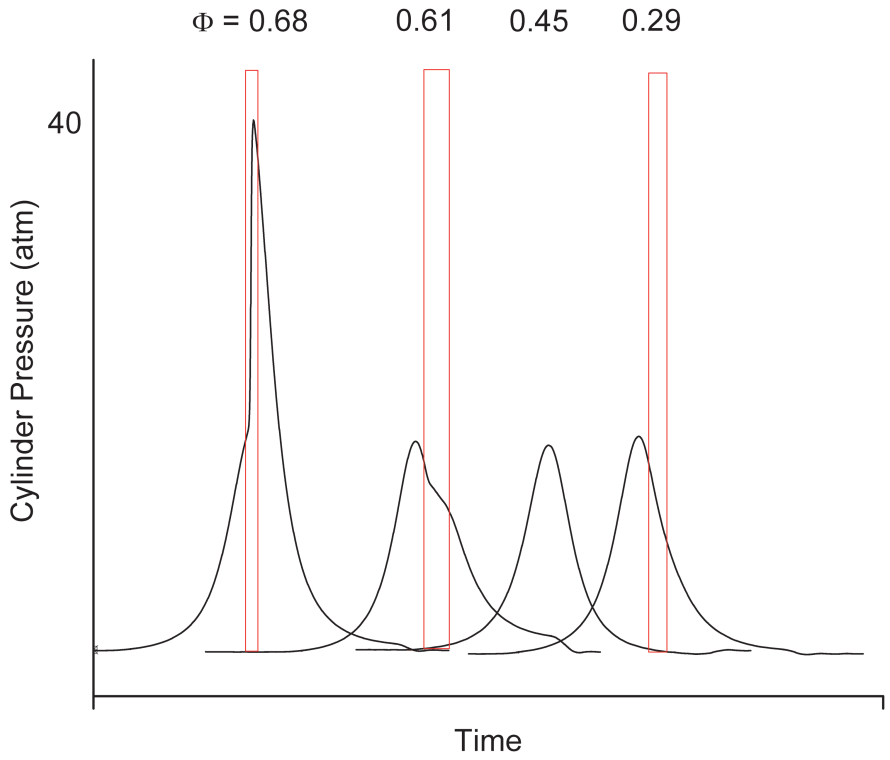

Figure 3.6: Typical pressure histories for engine conditions with iso-octane fuel. The data are superimposed for clarity. The boxed areas coincide with the imaging sequences of Figures 3.7 - 3.10.

Figures 3.7 - 3.10 show image sequences for HCCI combustion of iso-octane at various equivalence ratios. All images have been gain adjusted for clarity. All of the iso-octane images show blue emission originating in a localized area in the combustion chamber. The time required for the blue emission to expand from the point of origin to the remainder of the combustion chamber increased with leaner conditions. At $\phi =$ 0.68, relatively uniform blue emission consistently developed across the combustion chamber within four images (5.6 CAD) of the first indication of ignition, as shown in Fig. 3.7. The next leaner condition, $\phi = 0.61$, showed extreme signs of misfire through variation in cylinder pressure and in ignition imaging. Figure 3.8 shows the image sequence associated with one of the more frequently observed phenomena, with blue emission extending for 45 image frames (63 CAD). Other image sequences for $\phi = 0.61$, not shown, contained emission spanning between 32 frames (45 CAD) to 260 frames (364 CAD). Blue emission never appeared simultaneously throughout the volume of the combustion chamber for conditions leaner than $\phi = 0.68$.

As observed with some indolene conditions, the images obtained for iso-octane at $\phi = 0.68$ showed bright white emission (see Fig. 3.7), and again leaner conditions did not produce white emission. At the leanest conditions studied for iso-octane, ϕ = 0.29, blue emission was only occasionally observed during a cycle. Those cycles which did exhibit emission, indicated very weak intensities that appeared to travel throughout the cylinder for long times (see Fig. 3.10) for around 20-40 frames (30-55 CAD).

The rapid heat release rate for $\phi = 0.68$ noted in Fig. 3.6 corresponds temporally to the fully volumetric, intense blue emission seen in Fig. 3.7. Leaner conditions exhibited neither simultaneous volumetric blue emission nor high rates of heat release on the pressure traces.

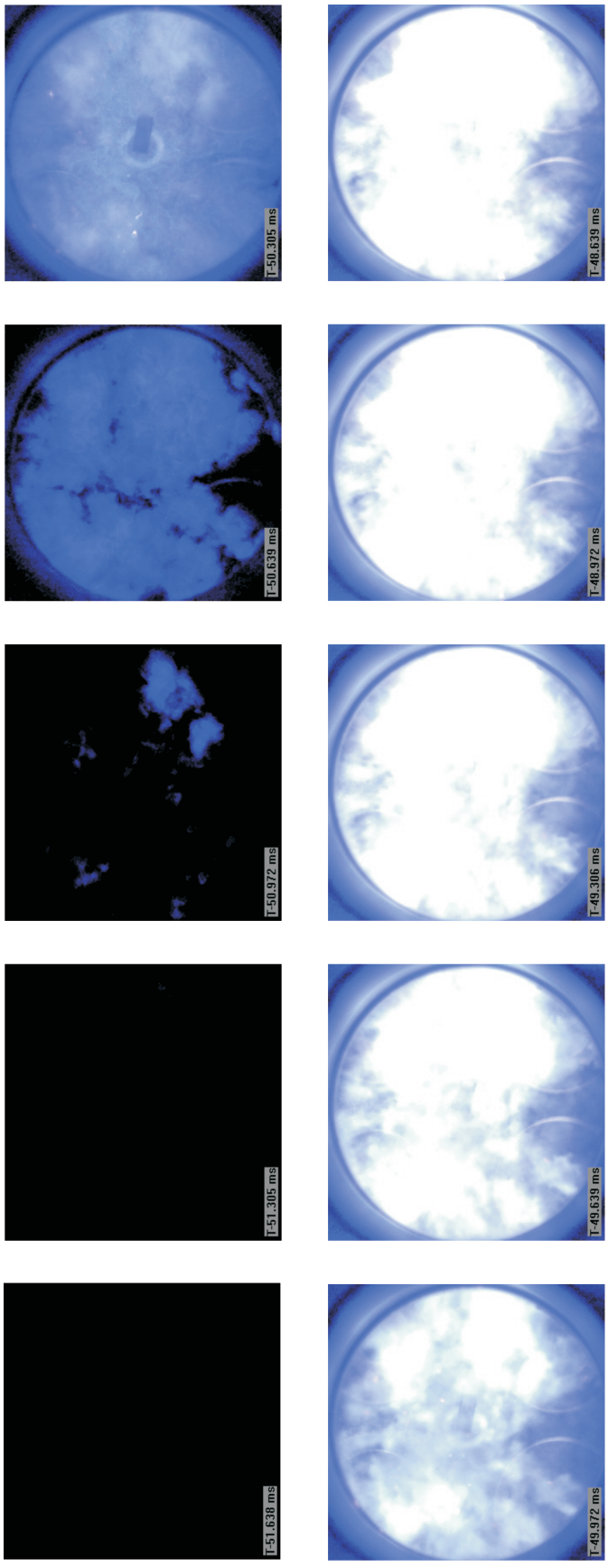

Figure 3.7: Image sequence for iso-octane at $\phi = 0.68$.

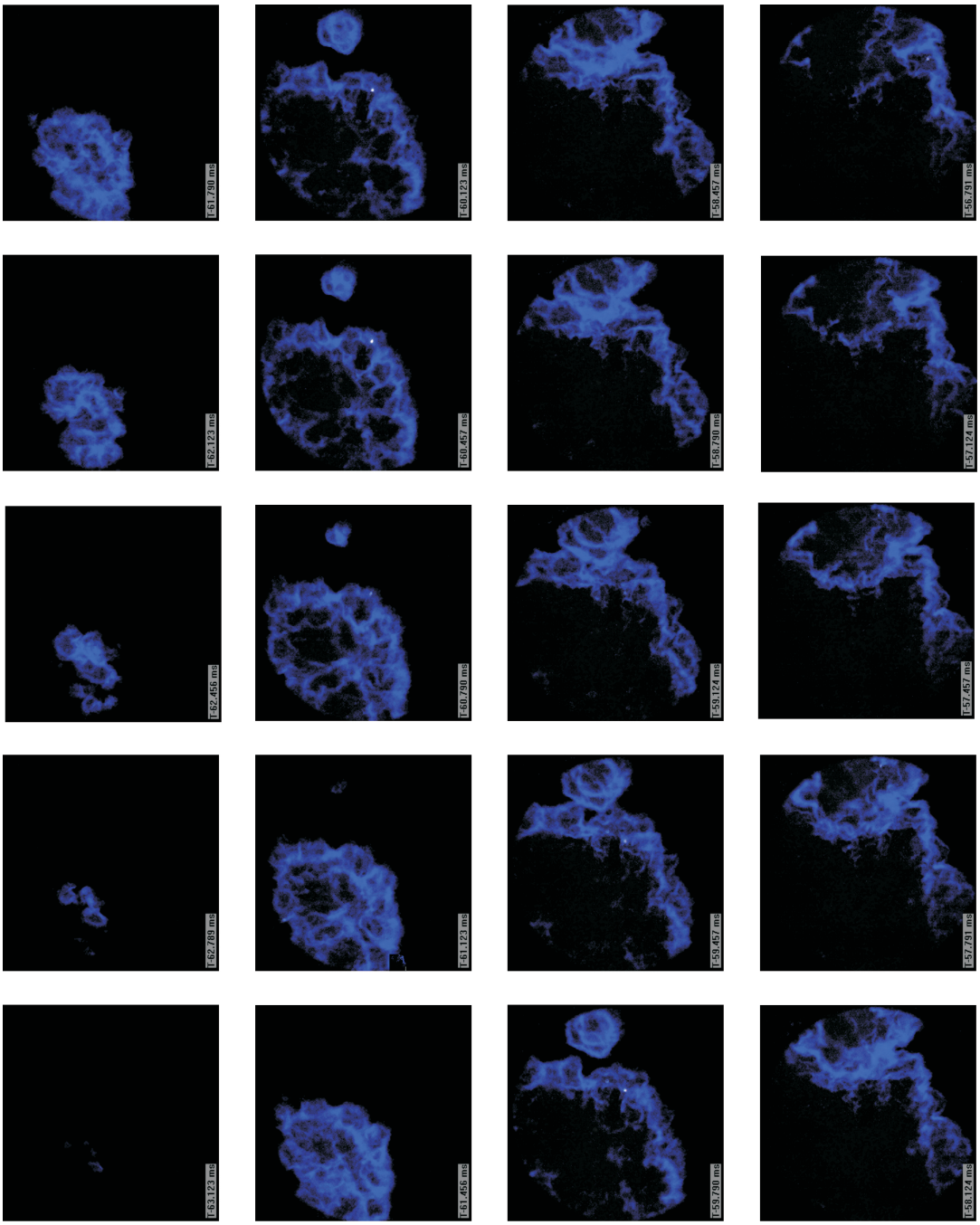

Figure 3.8: Image sequence for iso-octane at $\phi = 0.61$.

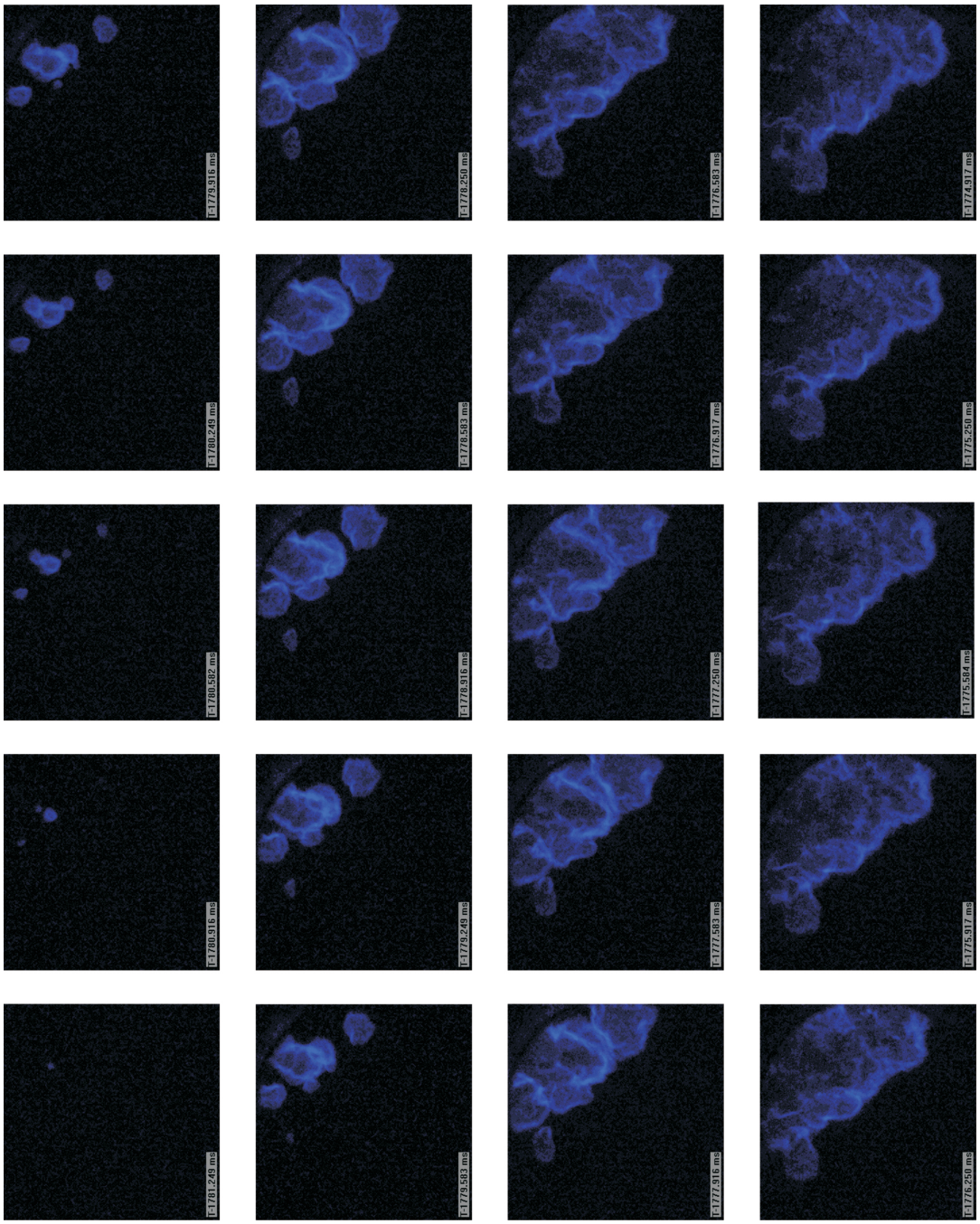

Figure 3.9: Image sequence for iso-octane at $\phi = 0.45$.

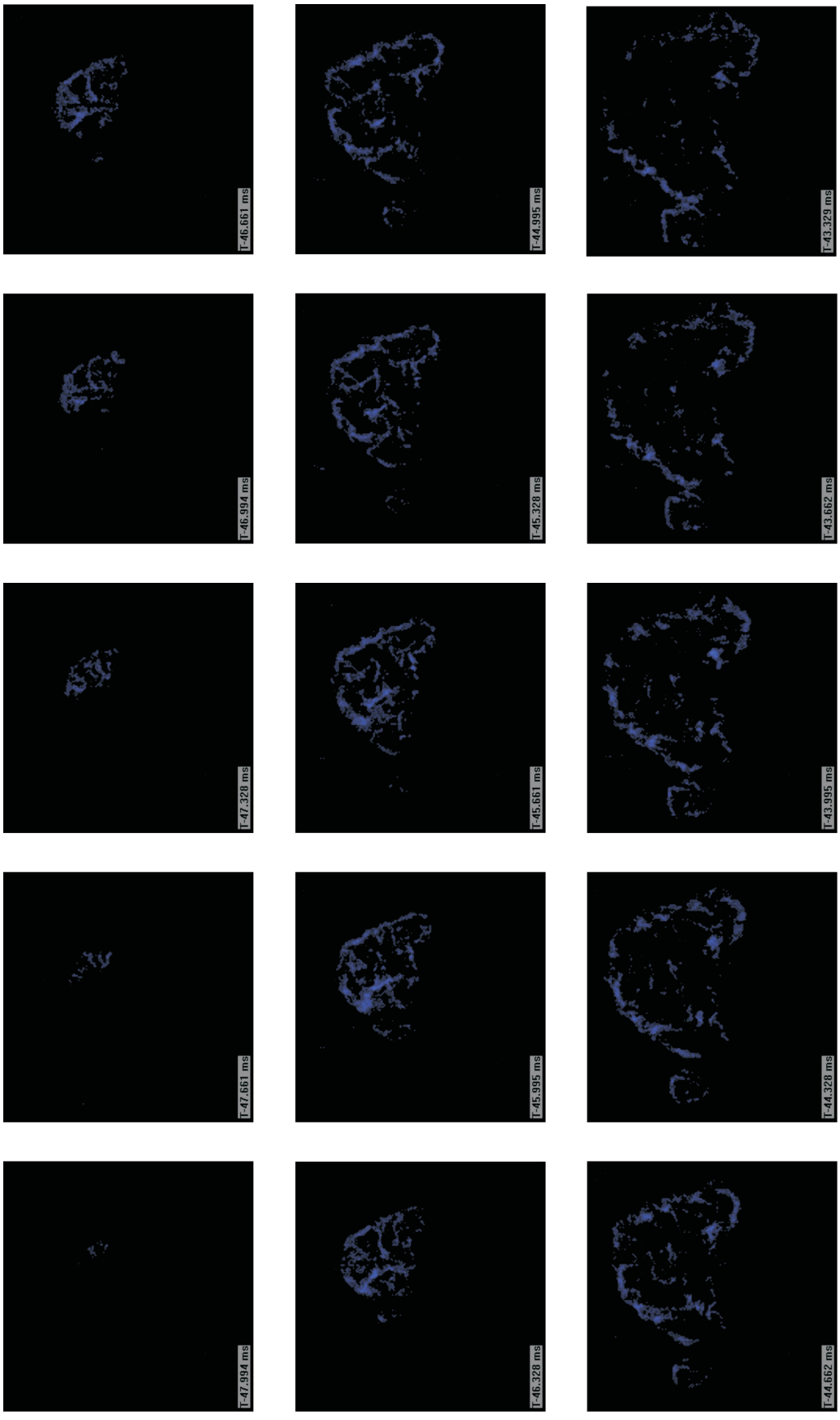

Figure 3.10: Image sequence for iso-octane at $\phi = 0.29$.

3.3.3 Gasoline

Examples of typical pressure traces for each gasoline run are shown in Figure 3.11. The image sequences shown in Figures 3.12 - 3.16 correlate to the pressure data, as presented in Fig. 3.11. All images have been gain adjusted for clarity. The pressure data showed ignition occurs during compression with high heat release rates for $\phi =$ 0.65. Leaner conditions at $\phi = 0.52$, 0.45, 0.37, and 0.29 showed ignition near TDC with decreasing heat release rates. The pressure data also showed increasing cycle-to-cycle variation in cylinder peak pressure with leaner fuel mixtures. Unlike the leanest iso-octane conditions, the ignition events for gasoline were always identifiable from the pressure data.

Figures 3.12 - 3.16 show image sequences for HCCI combustion of gasoline for decreasing equivalence ratios. Each of the gasoline sequences show blue emission originating in a localized area in the combustion chamber. As found with the higher equivalence ratios for the indolene and iso-octane fuels, the images obtained at $\phi =$ 0.65 showed bright white emission, after blue emission developed across the entire combustion chamber. Similar to the other fuels studied, the white emission was not observed at the leaner conditions. Gasoline exhibited behavior similar to indolene in the relationship between heat release rate and simultaneous volumetric blue emission; where higher rates of pressure rise correspond temporally to more intense, volumetric blue emission.

3.4 Discussion

As previously discussed in Chapter II, the visible blue emission recorded by the camera is attributed to C_2 or CH; each has strong emission bands in the blue (C_2:

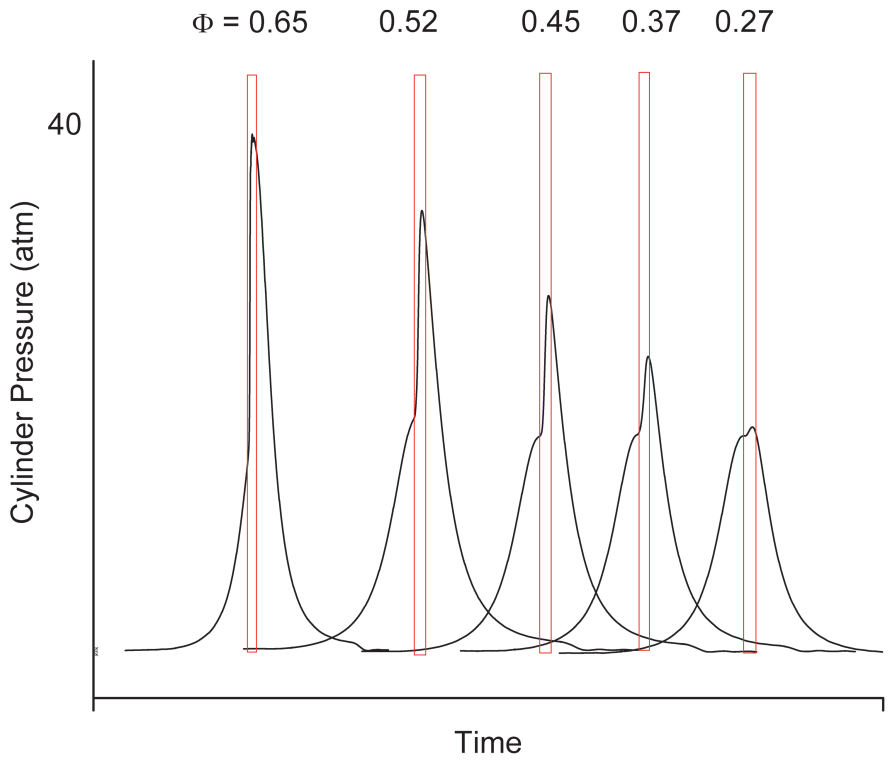

Figure 3.11: Typical pressure time histories for engine conditions with gasoline fuel. The data are superimposed for clarity. The boxed areas correspond to the imaging sequences of Figures 3.12 - 3.16.

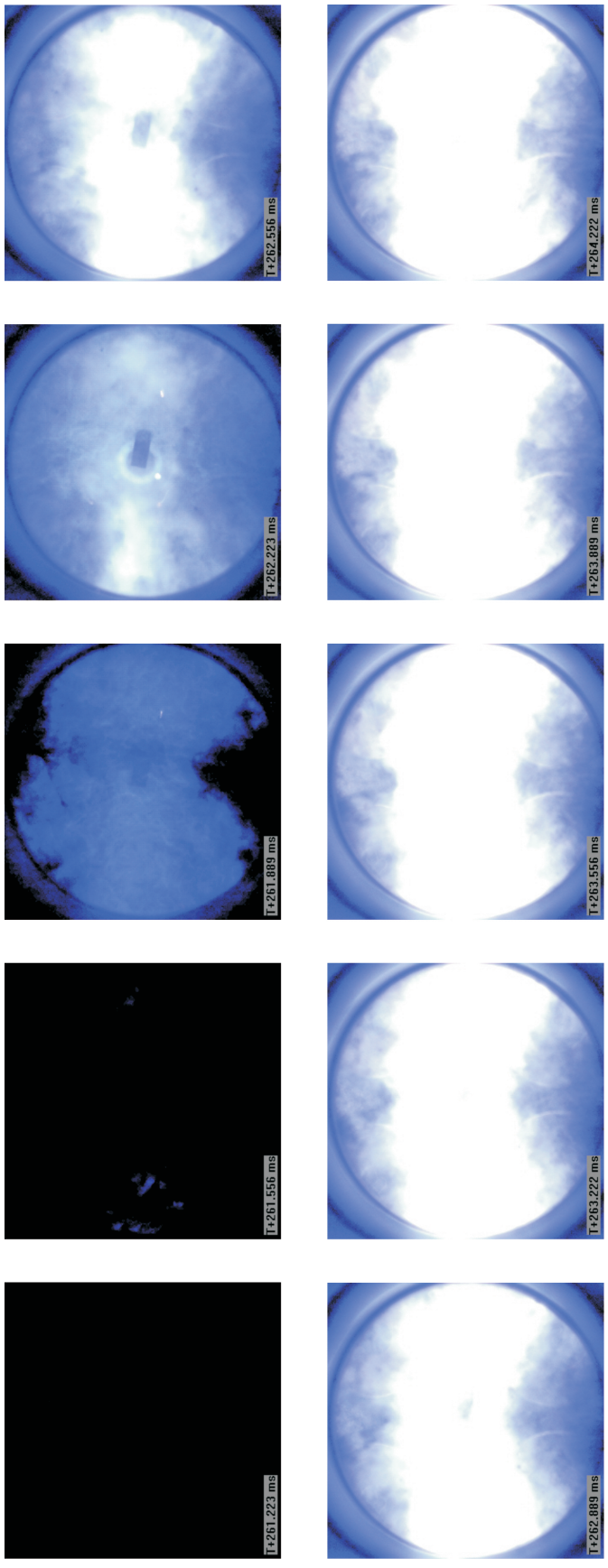

Figure 3.12: Image sequence for gasoline at $\phi = 0.65$.

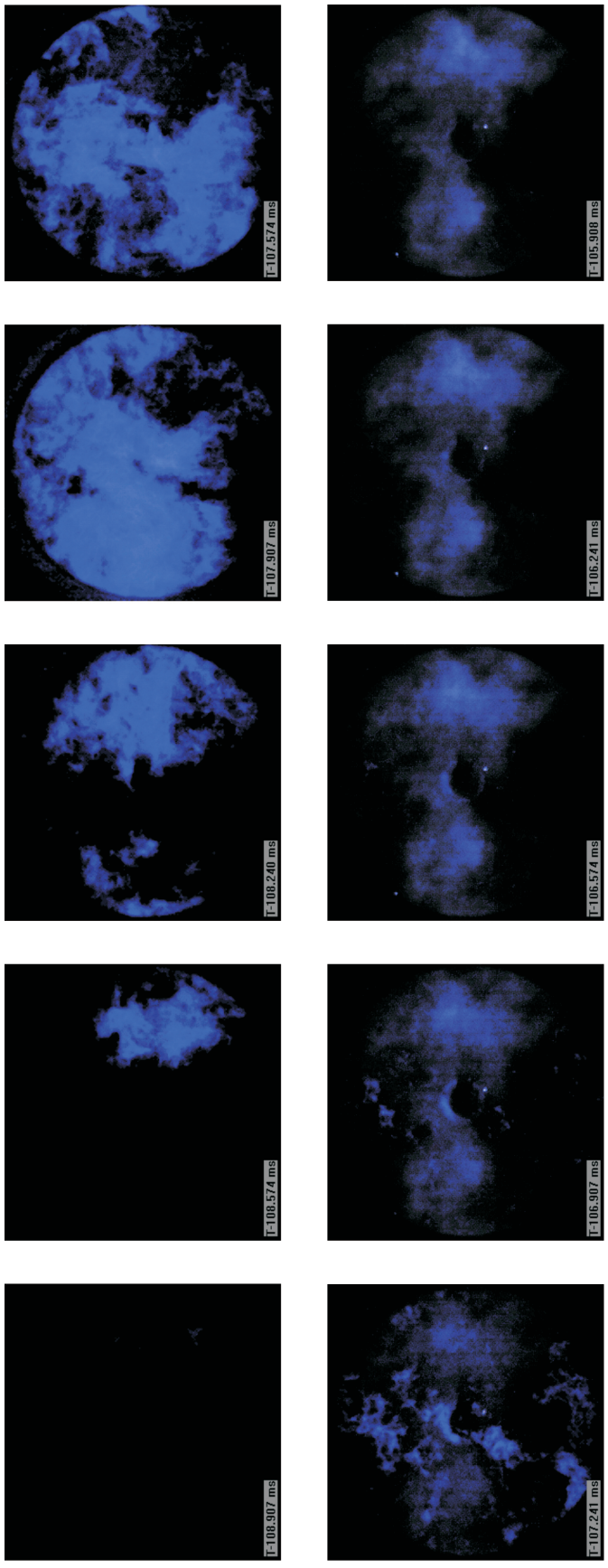

Figure 3.13: Image sequence for gasoline at $\phi = 0.52$.

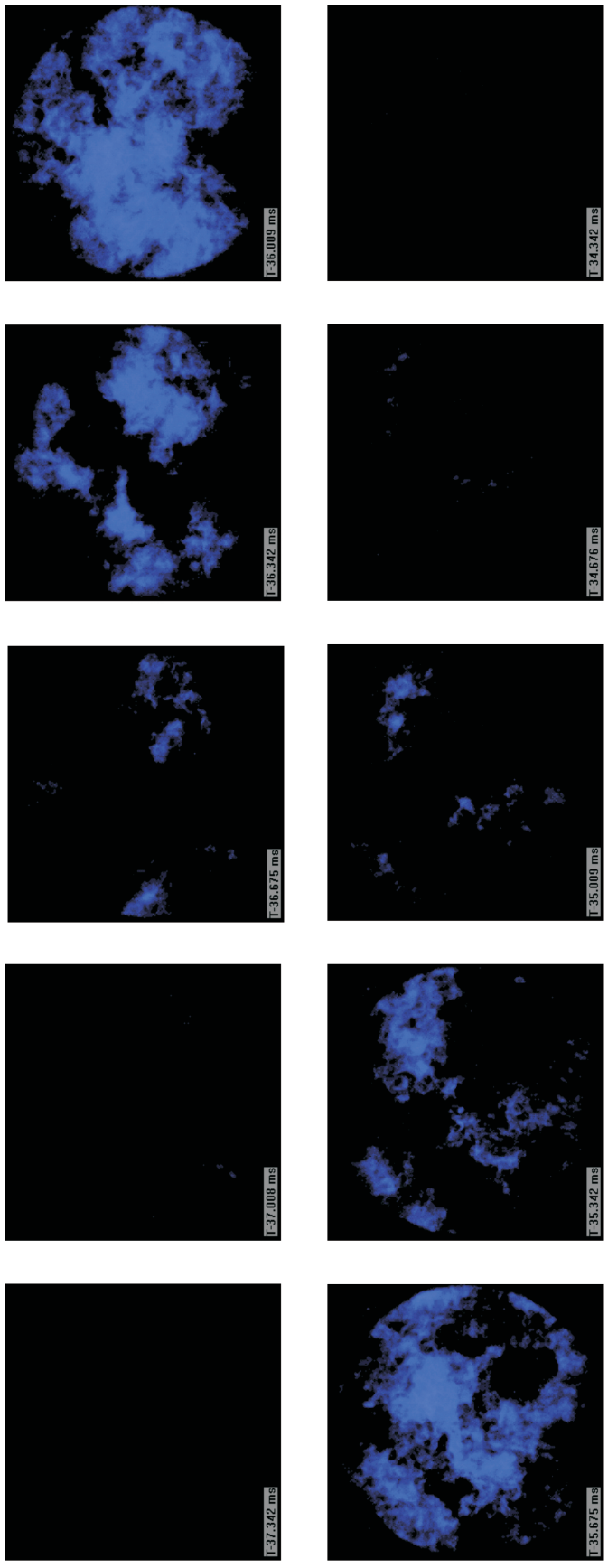

Figure 3.14: Image sequence for gasoline at $\phi = 0.45$.